Oscillations by symmetry breaking in homogeneous networks with electrical coupling

Yonatan Loewenstein and Haim Sompolinsky
Racah Institute of Physics and Center for Neural Computation, Hebrew University of Jerusalem, Jerusalem 91904, Israel
(Received 26 December 2001; published 24 May 2002)

In many biological systems, the electrical coupling of nonoscillating cells generates synchronized membrane potential oscillations. This work describes a dynamical mechanism in which the electrical coupling of identical nonoscillating cells destabilizes the homogeneous fixed point and leads to network oscillations via a Hopf bifurcation. Each cell is described by a passive membrane potential and additional internal variables. The dynamics of the internal variables, in isolation, is oscillatory, but their interaction with the membrane potential damps the oscillations and therefore constructs nonoscillatory cells. The electrical coupling reveals the oscillatory nature of the internal variables and generates network oscillations. This mechanism is analyzed near the bifurcation point, where the spatial structure of the membrane potential oscillations is determined by the network architecture and in the limit of strong coupling, where the membrane potentials of all cells oscillate in-phase and multiple cluster states dominate the dynamics. In particular, we have derived an asymptotic behavior for the spatial fluctuations in the limit of strong coupling in fully connected networks and in a one-dimensional lattice architecture.

DOI: 10.1103/PhysRevE.65.051926 PACS number(s): 87.18.Hf, 87.18.Pj, 87.18.Sn

I. INTRODUCTION

The dynamics of diffusively coupled excitable elements can often be surprising. In the early 1950s, Turing showed that the homogeneous fixed point of a network of identical elements, all at their stable fixed point, can be destabilized by diffusive coupling [1]. Since then, much experimental and theoretical work has shown that diffusion can break the spatial symmetry of the system and generate stationary waves via a pitchfork bifurcation [2]. However, the case of spatiotemporal symmetry breaking via a Hopf bifurcation has received little attention [3–5].

The dynamics of electrically coupled elements, which is a special case of diffusive coupling, is of particular interest. Electrical coupling between cells is very common in biological systems. These connections, which are called gap junctions, arise when special proteins on the membranes of adjacent cells align together to form a tunnel, which connects the cells and enables the diffusion of ions but not large proteins. Gap junctions have been demonstrated to connect cells in many tissues, including the cardiovascular system, the liver, lungs, kidneys, and pancreas. Electrical synapses are also common in the central nervous system, where they connect both glia cells and neurons. For example, electrical coupling has been demonstrated to connect inhibitory neurons in the cerebral and cerebellar cortices, hippocampal cells, photoreceptors and horizontal cells in the retina, and the neurons of the inferior olive. The dynamics of the neuronal networks both in the developmental stages and in the mature brain is strongly influenced by these connections [6].

Interestingly, in some of these biological systems, the membrane potential of the isolated cells is constant, but oscillates in the electrically coupled network, suggesting that electrical coupling is essential for the generation of oscillations. Recently we proposed a novel dynamic mechanism to explain these oscillations [7]. According to this mechanism, the spatiotemporal symmetry of the homogeneous stable state is broken when the electrical coupling destabilizes it, giving rise to oscillations via a Hopf bifurcation.

In this paper we generalize this mechanism, analyze the spatiotemporal structure of the oscillations near the bifurcation point and in the limits of strong coupling and fast membrane potential. We show that in this limit of strong coupling the dynamics of our mechanism resembles that of networks of globally inhibited and mutually inhibited oscillators. Using Van Der Pol oscillators, we demonstrate our dynamical mechanism and analyze two network architectures: a fully connected network and a one-dimentional lattice model.

II. MECHANISM FOR THE GENERATION OF NETWORK OSCILLATIONS

A. The isolated cell

Our starting point is that the dynamics of the isolated cell is described by the set of differential equations of the form

$$\dot{V} = -aV + bX, \tag{1}$$

$$\dot{X} = -V + A(X,Y),$$

$$\dot{Y} = B(X,Y),$$

where V is the membrane potential of the cell and (X,Y) is a state vector of two ''internal variables'' of the cell. These internal variables can represent, for example, the concentrations of different ions [7] or the membrane potential of other compartments of the cell [8]. First we assume that for the appropriate parameters a and b, Eq. (1) has a single fixed point (V^*,X^*,Y^*), which is globally stable, reflecting the fact that the isolated cell is not oscillating. Without loss of generality we assume that the fixed point of Eq. (1) is $(V^*=X^*=Y^*=0)$. Second we assume that the internal variables have a tendency to oscillate, i.e., when the voltage is affixed to its fixed point value $V=0$, the fixed point (0,0) of the equations

$$\dot{X}=A(X,Y), \tag{2}$$

$$\dot{Y}=B(X,Y),$$

is unstable and Eq. (2) has a single limit cycle attractor, which is globally stable. Under these conditions, the stability of the fixed point $(0,0,0)$ of Eq. (1) results from the negative feedback, which is provided by the interaction of the internal variables with the dynamics of the membrane potential.

From the above it follows that the stability matrix of the isolated cell dynamics, Eq. (1), at the zero fixed point

$$\underline{\underline{Q}}=\begin{bmatrix} -a & b & 0 \\ -1 & \dfrac{\partial A(0,0)}{\partial X} & \dfrac{\partial A(0,0)}{\partial Y} \\ 0 & \dfrac{\partial B(0,0)}{\partial X} & \dfrac{\partial B(0,0)}{\partial Y} \end{bmatrix} \tag{3}$$

is negative definite, whereas at least one of the eigenvalues of the stability matrix of the internal variables dynamics, Eq. (2), at its zero fixed point

$$\underline{\underline{Q'}}=\begin{bmatrix} \dfrac{\partial A(0,0)}{\partial X} & \dfrac{\partial A(0,0)}{\partial Y} \\ \dfrac{\partial B(0,0)}{\partial X} & \dfrac{\partial B(0,0)}{\partial Y} \end{bmatrix} \tag{4}$$

is unstable.

B. The network dynamics

We model a system of N identical elements of the type given by Eq. (1), which are electrically coupled via their membrane potential. The system dynamics is described by

$$\dot{V}_i=-aV_i+bX_i+\sum_{j=1}^{N} g_{ij}(V_j-V_i), \tag{5}$$

$$\dot{X}_i=-V_i+A(X_i,Y_i),$$

$$\dot{Y}_i=B(X_i,Y_i),$$

where $g_{ij}=g_{ji}\geqslant 0$ is the electrical coupling strength between the ith and jth cells.

Our main question is whether in such a system, increasing g_{ij} beyond a critical value will generate network oscillations despite the fact that the fixed point of the isolated cell is globally stable. We begin by showing the presence of oscillations in the limit of strong coupling and then we analyze the behavior near the bifurcation point.

C. The limit of strong coupling

To define the limit of strong coupling, we assume that $g_{ij}=g\tilde{g}_{ij}$, where $\tilde{g}_{ij}$ is of $O(1)$ and take the limit of $g\to\infty$. Summing the voltage dynamics term in Eq. (5) over all cells we obtain

$$\dot{V}=-aV+\frac{b}{N}\sum_{i=1}^{N} X_i, \tag{6}$$

$$\dot{X}_i=-V+A(X_i,Y_i)-\delta V_i,$$

$$\dot{Y}_i=B(X_i,Y_i),$$

where

$$V\equiv\frac{1}{N}\sum_{i=1}^{N} V_i, \tag{7}$$

$$\delta V_i\equiv V_i-V, \tag{8}$$

are the mean membrane potential across the network and the fluctuations, respectively. The dynamics of the fluctuations of the membrane potential is given by

$$\dot{\delta\vec{V}}=-a\,\delta\vec{V}+b\,\delta\vec{X}-g\underline{\underline{\tilde{G}}}\,\delta\vec{V}, \tag{9}$$

where the vector notation is over the N network cells

$$\delta X_i\equiv X_i-\frac{1}{N}\sum_{j=1}^{N} X_j, \tag{10}$$

and the matrix $\underline{\underline{\tilde{G}}}$ is defined by

$$\tilde{G}_{ij}\equiv\delta_{ij}\sum_{q=1}^{N}\tilde{g}_{iq}-\tilde{g}_{ij} \tag{11}$$

where δ_{ij} is the Kronecker delta function. Generally, $\underline{\underline{\tilde{G}}}$ has only one zero eigenvalue, which corresponds to the homogeneous eigenvector. The projection of $\delta\vec{X}$ on all the heterogeneous eigenvectors of $\underline{\underline{\tilde{G}}}$ is of $O(1)$. Thus, in the limit of $g\gg 1$ Eq. (9) becomes

$$\delta\vec{V}=\frac{b}{g}\,\underline{\underline{\tilde{G}}}^{-1}\delta\vec{X}+O\left(\frac{1}{g^2}\right) \tag{12}$$

and therefore, $\delta\vec{V}$ is of $O(1/g)$. Taking the limit of $g\to\infty$, the network dynamics, Eq. (5) becomes

$$\dot{V}=-aV+\frac{b}{N}\sum_{i=1}^{N} X_i, \tag{13}$$

$$\dot{X}_i=-V+A(X_i,Y_i),$$

$$\dot{Y}_i=B(X_i,Y_i).$$

The dynamics of the membrane potential V in Eq. (13) is only sensitive to perturbations of $\vec{X}$ in the homogeneous direction. Therefore, the fixed point is only stable in the homogeneous direction but is unstable to perturbations in the heterogeneous directions. This can be readily seen by linearizing Eq. (13) around the homogeneous zero fixed point. The eigenvalues of the stability matrix are the (stable)

eigenvalues of the stability matrix of the dynamics of the isolated cell around the zero fixed point $\underline{\underline{Q}}$, which correspond to the homogeneous direction and the eigenvalues of the stability matrix of the dynamics of the internal variables around the zero fixed point $\underline{\underline{Q'}}$, which correspond to the heterogeneous directions. Since by construction $\underline{\underline{Q'}}$ has at least one unstable eigenvector, the homogeneous zero fixed point of Eq. (13) is unstable.

Note that there are no stable homogeneous solutions to Eq. (13) because such a solution is described by the equations of the isolated cell, Eq. (1), which by construction has only one attractor, the zero fixed point. This implies that the symmetry between the different pairs $\{(X_i,Y_i)\}$ is necessarily broken in the asymptotic solution to Eq. (13). Thus, although the internal variables of the different cells ''see'' the same membrane potential, they respond to it differently. Therefore, the dynamics of the internal variables, with the driving force $V(t)$, in Eq. (13)

$$\dot{X}_i = -V(t) + A(X_i,Y_i), \tag{14}$$

$$\dot{Y}_i = B(X_i,Y_i),$$

has more than one asymptotic solution. Numerical simulations of Eq. (13) with several different models of internal variables show that for $N=2$, the internal variables of the two cells oscillate in antiphase, whereas the mutual membrane potential oscillates with double the frequency. When $N>2$, the dynamics exhibits many different limit cycle attractors, in which the activity of the internal variables of the different cells is clustered into two or more clusters, with different numbers of cells in each cluster. An example of this behavior is presented below.

Interestingly, Eq. (13) also describes the dynamics of N excitatory oscillatory cells (X_i,Y_i), which are all coupled via one inhibitory cell V. The dynamics of each of the oscillatory cells, in isolation, is described by Eq. (2), and each cell excites one global linear inhibitory cell with a coupling strength b/N. The latter inhibits each of the excitatory cells with a coupling strength of -1. When $N=1$, Eq. (13) reverts to Eq. (1) and the inhibitory cell suppresses the oscillations of the excitatory cell. However, when $N>1$, V exerts a global negative feedback, which suppresses the oscillations in the homogeneous direction but retains the instability in the heterogeneous direction. Indeed, the study of the dynamics of networks of excitatory neurons, all coupled to one global inhibitory cell has shown clustering of the excitatory cells similar to our results [9].

In general, $\underline{\underline{\tilde{G}}}$ has only one zero eigenvalue, which corresponds to the homogeneous eigenvector, and in the limit of $g\to\infty$, the network dynamics is independent of the details of the architecture. However, when $g\gg 1$ but $g<\infty$, the connectivity architecture influences the fluctuations in the membrane potential of the different cells, which are of $O(1/g)$. Taking only $O(1/g)$ elements in Eq. (12) and decomposing $\delta\vec{V},\delta\vec{X}$ in terms of the eigenvectors of $\underline{\underline{\tilde{G}}}$ we get

$$v^\mu = \frac{b}{g}\frac{x^\mu}{\tilde{G}^\mu}, \tag{15}$$

where v^μ, x^μ are the projections of the vectors $\delta\vec{V},\delta\vec{X}$, respectively, on the μth heterogeneous eigenvector of matrix $\underline{\underline{\tilde{G}}}$, and $\tilde{G}^\mu$ is the corresponding eigenvalue. In general $\delta\vec{X}$ is of $O(1)$, and up to corrections of $O(1/g)$ its dynamics is determined by Eq. (13). Therefore, it is reasonable to assume that $\delta\vec{X}$ is almost independent of the architecture and its projections on all the heterogenous eigenvectors of matrix $\underline{\underline{\tilde{G}}}$ are comparable. Therefore the spatial structure of the $O(1/g)$ membrane potential fluctuations, which are determined by Eq. (15), are dominated by the eigenvectors that correspond to the the smallest nonzero eigenvalues of $\underline{\underline{\tilde{G}}}$.

D. The bifurcation point

Above we have seen that the homogeneous zero fixed point $(V_i=X_i=Y_i=0)$ is stable in the absence of coupling, but is unstable in the limit of strong coupling. Here we investigate the bifurcation point, where the homogeneous fixed point is destabilized and oscillations emerge. Linearizing the network's dynamical equations, Eq. (5), around this homogeneous fixed point yields

$$\dot{V}_i = -aV_i + \sum_{j=1}^{N} g_{ij}(V_j - V_i) + bX_i, \tag{16}$$

$$\dot{X}_i = -V_i + \frac{\partial A(0,0)}{\partial X}X_i + \frac{\partial A(0,0)}{\partial Y}Y_i,$$

$$\dot{Y}_i = \frac{\partial B(0,0)}{\partial X}X_i + \frac{\partial B(0,0)}{\partial Y}Y_i.$$

It is convenient to represent the dynamical variables in terms of the eigenvectors of the connectivity matrix $\underline{\underline{G}} = g\underline{\underline{\tilde{G}}}$,

$$V_i = \sum_{\mu=1}^{N} v^\mu R_i^\mu, \tag{17}$$

$$X_i = \sum_{\mu=1}^{N} x^\mu R_i^\mu,$$

$$Y_i = \sum_{\mu=1}^{N} y^\mu R_i^\mu,$$

where $\{\vec{R}^\mu\}_{\mu=1}^N$ are the eigenvectors of $\underline{\underline{G}}$ with the corresponding eigenvalues $\{G^\mu\}_{\mu=1}^N$. Substituting Eq. (17) in Eq. (16) uncouples the different cells and Eq. (16) becomes

$$\frac{d}{dt}\begin{pmatrix} v^\mu \\ x^\mu \\ y^\mu \end{pmatrix} = \begin{bmatrix} -a-G^\mu & b & 0 \\ -1 & \dfrac{\partial A(0,0)}{\partial X} & \dfrac{\partial A(0,0)}{\partial Y} \\ 0 & \dfrac{\partial B(0,0)}{\partial X} & \dfrac{\partial B(0,0)}{\partial Y} \end{bmatrix} \begin{pmatrix} v^\mu \\ x^\mu \\ y^\mu \end{pmatrix}. \tag{18}$$

Equation (18) is, in fact, the linearized equation of an isolated cell around its zero fixed point, with an additional passive conductance G^μ. Thus, near the fixed point the system dynamics can be mapped into the dynamics of an isolated cell with additional ''stabilizing'' terms,

$$\dot{V} = -(a+G^\mu)V + bX, \tag{19}$$

$$\dot{X} = -V + A(X,Y),$$

$$\dot{Y} = B(X,Y).$$

Hence, the homogeneous fixed point of the system is destabilized by electrical coupling if and only if there exists eigenvalue G^μ such that the fixed point of Eq. (19) is unstable. The eigenvalue that corresponds to the homogeneous eigenvector of $\underline{\underline{G}}$ is $G^h=0$. Hence, instability can only arise in a heterogeneous direction. As we have seen above, in the limit of strong coupling, the homogeneous fixed point becomes unstable. This implies that for a sufficiently large G^μ, the zero fixed point of Eq. (19) is unstable. Thus, as the overall coupling strength is increased, instability arises when the largest eigenvalue of matrix $\underline{\underline{G}}$ exceeds a critical value G^c. Since the dynamics of Eq. (2) consists of an unstable fixed point and a stable limit cycle, the simplest scenario for the generation of the network instability is via a Hopf bifurcation. When the bifurcation is a normal Hopf, the frequency of the oscillations near the bifurcation is determined by the imaginary part of the conjugate eigenvalues of the stability matrix around the zero fixed point of Eq. (19), with $G^\mu = G^c$. Thus, near the bifurcation point, the frequency of the oscillations is only dependent on the properties of the isolated cell and is independent of the architecture. In contrast, the spatial structure of the oscillations near this bifurcation point is determined by the eigenvector, which corresponds to the largest eigenvalue of $\underline{\underline{G}}$. This eigenvector depends solely on the architecture of the electrical connections and is independent of the properties of the isolated cell. Note that matrix $\underline{\underline{G}}$ is real and symmetric and thus its eigenvectors are real. Therefore, if there is no redundancy in the largest eigenvalue, all cells will oscillate either in phase or in antiphase, depending on the corresponding eigenvector. In the case of $N=2$, there is only one heterogeneous eigenvector and the two cells will oscillate in an antiphase direction.

Thus, near the bifurcation point, the architecture of the network influences the dynamics of the network via the eigenvector, which corresponds to the largest eigenvalue. In contrast, in the limit of strong coupling, it is the eigenvectors that correspond to the smaller eigenvalues that contribute more to the dynamics of the network.

E. The limit of fast membrane dynamics

Our mechanism requires that the membrane potential suppresses the oscillations of the internal variables in the isolated cell by exerting a negative feedback. This can also be achieved if the dynamics of the membrane potential is instantaneous. Changing the time constant of the membrane in Eq. (1) is equivalent to changing a,b while keeping the ratio b/a constant. In the limit of fast membrane dynamics, the membrane potential follows its fixed point equations, and Eq. (5) becomes

$$\dot{\vec{X}} = -b(\underline{\underline{G}}+a\underline{\underline{I}})^{-1}\vec{X} + \vec{A}(X_i,Y_i), \tag{20}$$

$$\dot{\vec{Y}} = \vec{B}(X_i,Y_i),$$

where $A_i \equiv A(X_i,Y_i)$ and $B_i \equiv B(X_i,Y_i)$. When $N=1$, Eq. (20) describe the dynamics of the isolated variables with an extra negative feedback term for variable X of strength b/a. If $\underline{\underline{Q'}}$ and b/a are such that $\mathrm{tr}(\underline{\underline{Q'}}) < b/a < [\|\underline{\underline{Q'}}\|/\partial\bar{B}(0,0)/\partial Y]$, then for $N=1$, this negative feedback will stabilize the fixed point. However, when $N>1$, diagonalizing Eq. (20) around the homogeneous fixed point reveals that whereas the strength of the negative feedback in the homogeneous direction remains b/a, it decreases to $b/(a+G^\mu)$ in the heterogeneous directions, where G^μ are the eigenvalues of $\underline{\underline{G}}$ that correspond to these directions. For large enough G^μ, this negative feedback is too weak to suppress fluctuations and the homogeneous zero fixed point is no longer stable. This bifurcation takes place for $G^c = b/\mathrm{tr}(\underline{\underline{Q'}}) - a$, and the simplest scenario is a Hopf bifurcation, which leads to oscillations.

In the limit of strong coupling, in general $[(\underline{\underline{G}}+a\underline{\underline{I}})^{-1}]_{ij} \to 1/aN$ and Eq. (20) yields

$$\dot{X}_i = -\frac{b}{a}\frac{1}{N}\sum_{j=1}^{N} X_j + A(X_i,Y_i), \tag{21}$$

$$\dot{Y}_i = B(X_i,Y_i),$$

which represents the dynamics of N oscillators that mutually inhibit each other. Numerical simulations of Eq. (21) with different nonlinear models show similar clustering behavior to those observed with the dynamics of Eq. (13). Similar results have been observed in the study of the dynamics of networks of cells, mutually coupled with inhibitory synapses [10].

III. ELECTRICALLY COUPLED MODEL WITH A Van Der Pol OSCILLATOR

A. The model

Our mechanism can be realized with different nonlinearities of the internal variables. Here we demonstrate it in a model where the dynamics of the internal variables, Eq. (2), is described by a Van der Pol oscillator [11],

$$\dot{X} = -Y + 0.4X(5+Y-Y^2), \tag{22}$$

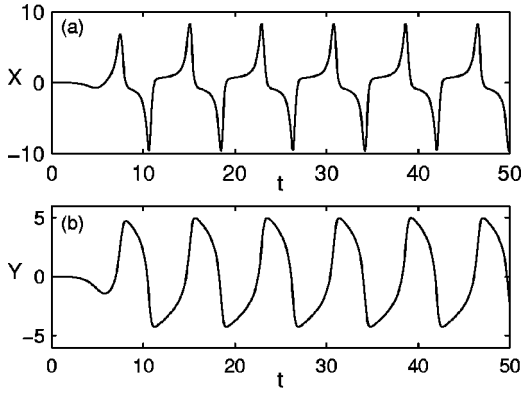

FIG. 1. Oscillations of the internal variables. The zero fixed point of Eq. (22) is unstable and the dynamics converges to limit cycle oscillations (a), in X and (b) in Y.

$$\dot{Y}=X.$$

These equations have one fixed point at (0,0). Linear stability analysis reveals that this fixed point is unstable, and numeric simulations show that these equations have only one attractor, which is a limit cycle (Fig. 1).

The isolated cell is generated by linear coupling one of the internal variables X to a passive membrane potential V, yielding

$$\dot{V}=-aV+bX, \tag{23}$$

$$\dot{X}=-V-Y+0.4X(5+Y-Y^2),$$

$$\dot{Y}=X,$$

where $a,b\geqslant 0$ are parameters.

Linearizing Eq. (23) around the fixed point (0,0,0) and applying the Routh-Hurwitz condition, we find that the fixed point is stable if and only if $b>8$ and $(b+4-\sqrt{b^2-8b})/4 < a < (b+4+\sqrt{b^2-8b})/4$.

Figure 2 shows the dynamics of Eq. (23) with $a=3$; $b=10$. In contrast to the unstable zero fixed point and the stable limit cycle of Eq. (22) shown in Fig. 1, the zero fixed point of Eq. (23) is stable and numeric simulations suggest that it is also globally stable, in agreement with the requirements of our mechanism as described above.

B. The bifurcation point

The dynamics of the electrically coupled network is described by

$$\dot{V}_i=-aV_i+bX_i+\sum_{j=1}^{N} g_{ij}(V_j-V_i), \tag{24}$$

$$\dot{X}_i=-V_i-Y_i+0.4X_i(5+Y_i-Y_i^2),$$

$$\dot{Y}_i=X_i.$$

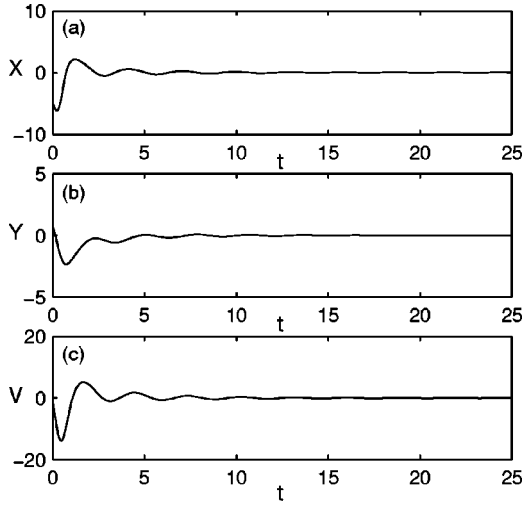

FIG. 2. The isolated cell is not oscillating. The zero fixed point of Eq. (23) is stable and after a perturbation the internal variables (a), X and (b), Y and (c), the membrane potential V converge to the zero fixed point.

In order to investigate the effect of the electrical coupling on the dynamics of the network it is useful to analyze the stability of the homogeneous zero fixed point. Linearizing Eq. (24) around its zero fixed point and applying the Routh-Hurwitz condition reveals that the fixed point is unstable if and only if the largest eigenvalue of the connectivity matrix $\underline{\underline{G}}$ exceeds the critical value $G^c=(1+\sqrt{5})/2$, and the type of bifurcation is Hopf. Figure 3 illustrates the dynamics of Eq. (24) near the bifurcation point, where the largest eigenvalue of the connectivity matrix $\underline{\underline{G}}$ is equal to $G^c+0.02$. Numerical simulations show that the bifurcation is a normal Hopf and thus, the spatial structure of the asymptotic solution near the bifurcation point is determined by the eigenvector that corresponds to the largest eigenvalue. When $N=2$, the direction of the heterogeneous eigenvector of $\underline{\underline{G}}$ is $(1,-1)$. This antiphase structure of the oscillations is shown in Fig. 3(a) for $N=2$. When the number of cells is larger, the relative phases and amplitudes of the membrane potential oscillations of the different cells is determined by the connectivity architecture. This is illustrated in Figs. 3(b)–3(c) for $N=4$. In Fig. 3(b), cells 2–4 are connected to the first cell with the same coupling strength, and therefore the oscillations closely follow the eigenvector $(3,-1,-1,-1)$, which corresponds to the largest eigenvalue of the connectivity matrix $\underline{\underline{G}}$. In contrast, the connectivity of the cells in Fig. 3(c) is a nearest neighbor along a line with equal coupling strength. In this case the eigenvector $(1,-1-\sqrt{2},1+\sqrt{2},-1)$ corresponds to the largest eigenvalue of the connectivity matrix $\underline{\underline{G}}$ and this is reflected in the spatiotemporal structure of the oscillations.

C. Infinite coupling

In the limit of infinitely strong coupling, the membrane potentials of the different cells are equal and their dynamics is determined by the dynamics of the mean membrane potential. Thus, Eq. (24) is reduced to

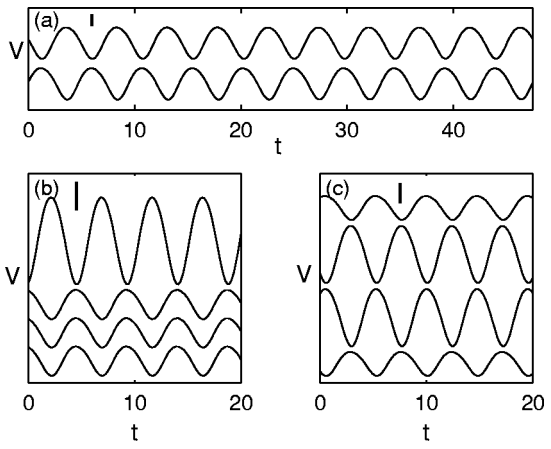

FIG. 3. Network oscillations near the bifurcation point. Simulating Eq. (24) with the largest eigenvalue of the connectivity matrix $\underline{\underline{G}}$ being equal to $G^c+0.02$ shows that the spatial structure of the membrane potential oscillations is determined by the eigenvector that corresponds to the largest eigenvalue. (a) $N=2$: The two consecutive traces represent the time course of the membrane potential oscillations of the two cells with connectivity of $g=0.819$. The only nonzero eigenvalue of $\underline{\underline{G}}$ corresponds to the heterogeneous eigenvector $(-1,1)$. This is reflected in the antiphase shape of the membrane potential oscillations. (b) The four consecutive traces represent the time course of the membrane potential oscillations of cells 1–4 (top to bottom) in a network where $N=4$. In this network, cell 1 is connected to cells 2–4 with a coupling strength of $g=0.4095$. The eigenvector, which corresponds to the largest eigenvalue of the connectivity matrix $\underline{\underline{G}}$, is $(3,-1,-1,-1)$, and the membrane potential oscillations of the four cells closely follow this eigenvector. (c) Identical to (b) with a different connectivity matrix. Here the four cells are placed along a straight line with nearest neighbors coupling strength of $g=0.4798$. The eigenvector that corresponds to the largest eigenvalue is $(1,-1-\sqrt{2},1+\sqrt{2},-1)$ and this is reflected in the shape of the membrane potential oscillations. The size of the vertical bar in (a)–(c) is 0.5.

$$\dot{V}=-aV+\frac{b}{N}\sum_{i=1}^{N}X_i, \tag{25}$$

$$\dot{X}_i=-V-Y_i+0.4X_i(5+Y_i-Y_i^2),$$

$$\dot{Y}_i=X_i.$$

Since the homogeneous solution of Eq. (25) is unstable, the symmetry between the different cells is broken and the asymptotic solution is heterogeneous. Numerical simulations show that in these solutions the internal variables group into several clusters. The internal variables within each cluster oscillate in phase but not in phase with those of the cells in other clusters. The type of symmetry breaking determines the number of such different heterogeneous solutions, all with the same shape of the common membrane potential oscillations but each with different cells having a different phase of internal variables oscillations. This is illustrated in Fig. 4, where Eq. (25) is simulated with $N=4$. In Figs. 4(a1) and 4(b1) the values of X for the four cells is shown as a function

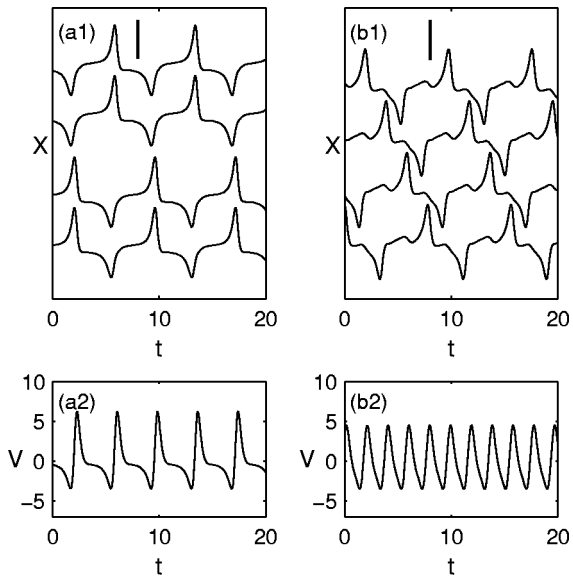

FIG. 4. Clustering of network oscillations in the limit of strong coupling. Simulating Eq. (25) with $N=4$ results in two types of asymptotic solutions depending on the initial conditions. (a) Clustering into two clusters. (a1) The four consecutive traces represent the time course of X for the four cells. The internal variables group into two clusters of two cells $[(1,2),(3,4)]$, where oscillations within a cluster are in-phase but are in antiphase with the oscillations of the other cluster. This is reflected in the shape of the common membrane potential V. (a2) An increase in X in one of the clusters generates an increase in V. Thus, the frequency of membrane potential oscillations is double that of the internal variables. (b) Clustering into four clusters. (b1) Different initial conditions result in a different asymptotic solution. In this case, the internal variables of each of the cells oscillate out of phase with respect to all other cells. (b2) An increase in X in one of the cells generates a smaller increase in V, and the frequency of membrane potential oscillations is four times that of the internal variables. Note that the time courses of the internal variables oscillations, (a1) and (b1) are very similar to the oscillations of X in Fig. 1(a), where there was no interaction with membrane potential. The size of the vertical bar in (a1) and (b1) is 10.

of time and in Figs. 4(a2) and 4(b2) their common membrane potential is shown as a function of time. In Fig. 4(a1), the internal variables of the cells cluster into two clusters of two cells: $[(1,2),(3,4)]$. The existence of these two clusters is reflected in the spatiotemporal structure of the membrane potential oscillations, Fig. 4(a2). An increase in X in one of the clusters generates an increase in V, and thus the frequency of membrane potential oscillations is double the frequency of the internal variables oscillations. This type of symmetry breaking implies that there exist two additional stable asymptotic solutions with the same membrane potential oscillations but with different clustering pairs of the internal variables: $[(1,3),(2,4)],[(1,4),(2,3)]$. In addition to these solutions, numerical simulations show that this system exhibits another type of typical symmetry breaking. This solution, which is characterized by a different clustering solution is illustrated in Fig. 4(b). In Fig. 4(b1), the internal variables of all four cells oscillate out of phase with respect

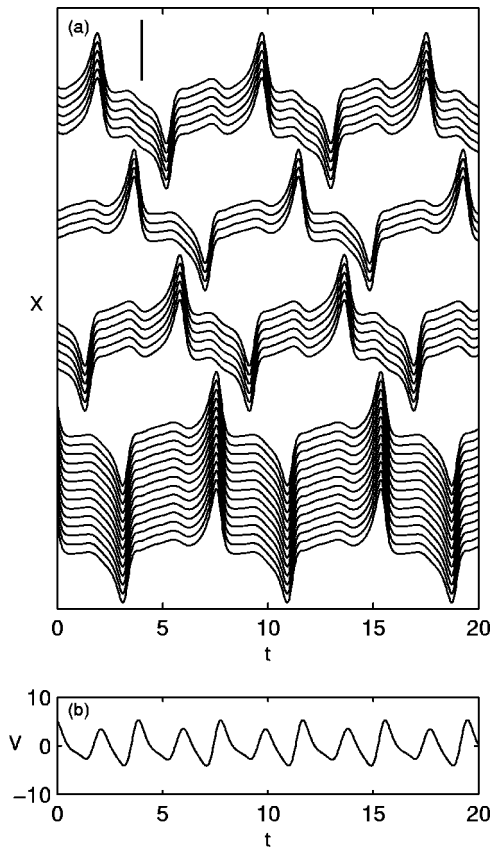

FIG. 5. Clustering of network oscillations in a large network. Simulating Eq. (25) with $N=500$ typically results here in the formation of three to four clusters. (a) The time courses of X for 30 randomly chosen cells show clear clustering into four clusters of varying sizes. (b) This clustering is reflected in the shape of the common membrane potential V. An increase in X in one of the clusters generates an increase in V, and the amplitude of the increase is dependent on the number of cells in the cluster. The size of the vertical bar in (a) is 10.

to all other internal variables. Thus, the frequency of the membrane potential oscillations, Fig. 4(b2), is four times that of the internal variables. This type of symmetry breaking generates five additional solutions, all with the same structure of membrane potential oscillations but with a different ordering of the internal variables.

We have simulated large networks of up to 500 cells in the limit of infinitely strong coupling. The asymptotic solution to Eq. (25) with $N=500$ depends on the initial conditions, and typically, the network forms three to four clusters, where the number of cells in each cluster differs. This is illustrated in Fig. 5: the internal variables X of 30 randomly chosen cells are shown in Fig. 5(a) and the common membrane potential is shown in Fig. 5(b). The oscillations of the internal variables in Fig. 5(a) show clear clustering into four clusters. An increase in X in one of the clusters corresponds to an increase in V, Fig. 5(b), and the amplitude of this increase is monotonous with the number of cells in the cluster. Thus, the detailed shape of the common oscillating potential bears a signature of the clustering structure of the internal variables.

D. Strong coupling

When the coupling is finite, the network dynamics is dependent on the connectivity architecture and on the coupling strength. Here we analyze how the coupling strength influences the network behavior in the strong coupling regime for two network architectures: fully connected network and one-dimensional lattice (also known as the ''ring model'').

1. Fully connected network

Here we analyze the dynamics of a network where all cells are coupled to all the other cells with the same coupling strength g. In this case the connectivity matrix $\underline{\underline{G}}$ has one zero eigenvalue, which corresponds to the homogeneous direction and $N-1$ eigenvalues, all equal to gN, which correspond to the heterogenous directions. Hence, the proper scaling of the coupling strength is $g=\bar{g}/N$. How does the size of $\bar{g}$ influence the network dynamics? Numerical simulations show that the existence of several nontrivial clustering solutions, which are seen in the infinite coupling regime, is retained even when $\bar{g}$ is of $O(1)$. This behavior is illustrated in Fig. 6, where Eq. (24) is simulated for a fully connected network with $N=4$ and $\bar{g}=32$. In Fig. 6(a), the cells are clustered into two clusters of two cells, similar to Fig. 4(a) whereas in Fig. 6(b) the cells are grouped into four clusters, similar to Fig. 4(b). The main effect of having *finite g*, is the presence of spatial fluctuations in the membrane potential, as is evident in Figs. 6(a2) and 6(b2) [compare with Figs. 4(a2) and 4(b2)]. In the limit of strong coupling, these spatial fluctuations are determined by Eq. (15). Since all nonzero eigenvalues of $\underline{\underline{G}}$ are equal to $\bar{g}$, in the limit of $\bar{g}\gg 1$, the membrane potential fluctuations are determined by

$$\Delta V \equiv \sqrt{\left\langle \frac{1}{N}\|\delta\vec{V}\|^2 \right\rangle} = \frac{b}{g}\sqrt{\left\langle \frac{1}{N}\|\delta\vec{X}\|^2 \right\rangle}. \qquad (26)$$

Here $\delta\vec{X}$ is determined by the clustering configuration and is of $O(1)$ with corrections that are of $O(1/g)$. This is illustrated in Fig. 7 that shows the standard deviation of the fluctuations, averaged over the four cells and over 200 time units as a function of $1/\bar{g}$. Similar to Figs. 4 and 5, different initial conditions could result in clustering into two clusters (denoted here by crosses) or four clusters (denoted here by boxes). Note that each clustering solution forms a straight line with a different slope, reflecting the different shape of $\vec{X}$ in the asymptotic solution.

2. One-dimensional lattice

The dependence of the fluctuations in V on the coupling strength in a one-dimensional lattice model is more complex. Here we analyze a model in which each cell is coupled to its two nearest neighbors with equal coupling strength g with periodic boundary conditions. The eigenvectors of the connectivity matrix $\underline{\underline{G}}$ in this model are the Fourier modes, and the eigenvalues are $G^k=2g([1-\cos(2\pi k/N)]$, $k=1,\ldots,N$. Thus, in the thermodynamical limit, when $N\to\infty$, the eigen-

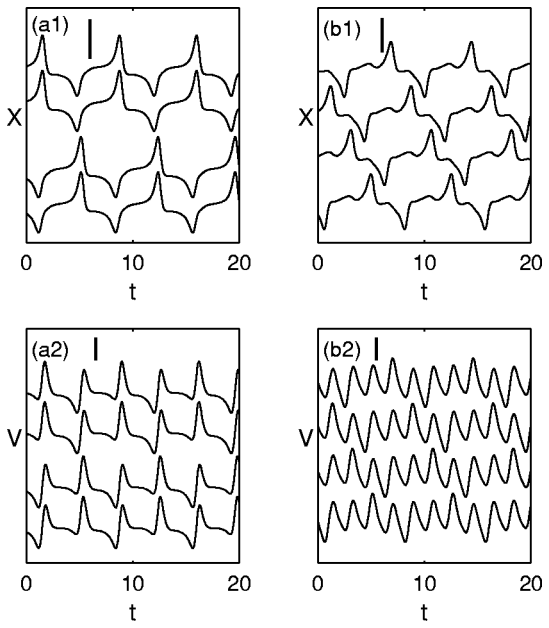

FIG. 6. Clustering of network oscillations with moderate coupling. Simulating Eq. (24) with $N=4$ and a connectivity architecture of all to all with $\bar{g}_{i\neq j}=32$ reveals similar patterns to Fig. 4. (a) Clustering into two clusters. (a1) The four consecutive traces represent the time course of X of the four cells. The internal variables group into two clusters of two cells, similar to Fig. 4(a1). (a2) The membrane potentials of the four cells. Note that an increase in X in one cluster generates an increase in V in the cells in that cluster, and a smaller increase in V in the cells of the other cluster, which is induced via the electrical connections. (b1) Different initial conditions result in a different asymptotic solution. In this case, the internal variables of each of the cells oscillate out of phase with respect to all other cells, similar to Fig. 4(b1). This is reflected in the shape of the membrane potential oscillations of the different cells (b2). An increase in X in one of the cells generates an increase in V in the corresponding cell, and a smaller increase in V in all the other cells. The size of the vertical bar in (a1) and (b1) is 10 and in (a2) and (b2) is 5.

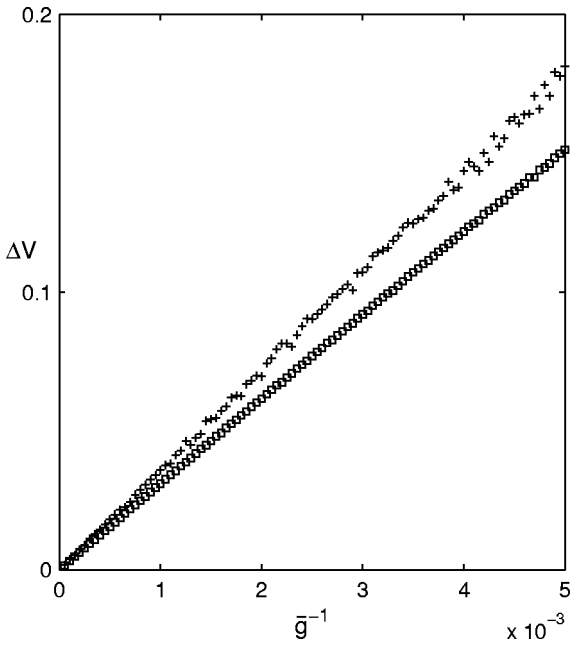

FIG. 7. The spatial fluctuations in the membrane potential as a function of the coupling strength in a fully connected network. Equation (24) is simulated with $N=4$ and $g_{i\neq j}=\bar{g}/N$ for different values of $\bar{g}$. The fluctuations were calculated by computing $\Delta V \equiv \sqrt{\langle \delta V^2 \rangle}$, where the mean is taken over the four cells and over 200 time units. Crosses represent events in which the initial conditions resulted in grouping of the cells into two clusters, similar to Figs. 4(a) and 6(a) and the boxes represent events in which the initial conditions resulted in grouping of the cells into four clusters, similar to Figs. 4(b) and 6(b). Each type of asymptotic solution forms a straight line, with a different slope in agreement with Eq. (15). The different slope results from the different shape of $\vec{X}$ in the asymptotic solution.

values with small values of k are small even when $g \gg 1$. Thus, the fluctuations in the membrane potential cannot be approximated by Eq. (15). Rewriting Eq. (9) in the spatial and temporal Fourier space we obtain

$$v^k(\omega)=\frac{bx^k(\omega)}{a+G^k-i\omega b}, \tag{27}$$

where $v^k(\omega)$ and $x^k(\omega)$ are the Fourier coefficients of the membrane potential $\vec{V}(t)$ and the internal variables $\vec{X}(t)$, respectively. Using Parseval's theorem, the mean spatial fluctuation of the membrane potential is

$$\Delta V=\sqrt{\frac{1}{N}\sum_{k=1}^{N-1}\int d\omega |v^k(\omega)|^2}. \tag{28}$$

Next we assume that $x^k(\omega)$ is only weakly dependent on k. Indeed, numerical simulations show that for $g,N \gg 1$, $\vec{X}$ has a considerable projection on all the eigenvectors of $\underline{\underline{G}}$. Thus, since $g \gg 1$, most of the contribution to ΔV comes from the small k, and ΔV can be written as

$$\Delta V \propto \sqrt{\frac{1}{\sqrt{g}}\int_{2\pi\sqrt{g}/N}^{\infty} dq \int d\omega \left| \frac{x\left(\frac{q}{\sqrt{g}},\omega\right)}{a+q^2-i\omega b}\right|^2}. \tag{29}$$

Most of the contribution to the integral over q comes from $q=O(1)$. Thus, assuming that $x(s,\omega)$ is smooth with respect to s, we approximate Eq. (29) by

$$\Delta V \propto \sqrt{\frac{1}{\sqrt{g}}\int_{2\pi\sqrt{g}/N}^{\infty} dq \int d\omega \left| \frac{x(0,\omega)}{a+q^2-i\omega b}\right|^2}. \tag{30}$$

Equation (30) determines the scaling behavior of ΔV in the limit of large N and g. We first consider the themodynamic limit, where the limit of large g is taken after the $N\to\infty$ limit. In this case, the lower limit of the integral goes to zero and Eq. (30) yields

$$\Delta V \propto g^{-1/4}. \tag{31}$$

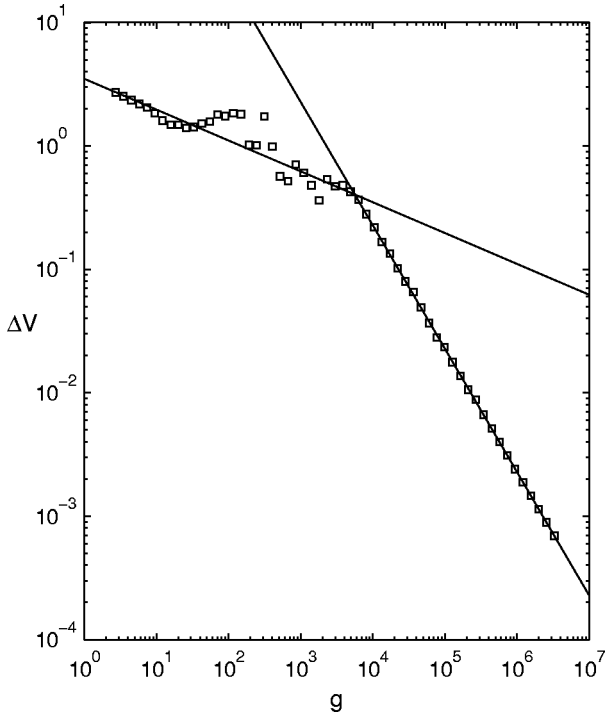

FIG. 8. The spatial fluctuations in the membrane potential as a function of the coupling strength in a one-dimensional nearest neighbor lattice model. Equation (24) is simulated with $N=200$ and $g_{ij}=g(\delta_{i,j+1}+\delta_{i,j-1})$ and periodic boundary conditions. The value of g is initially set to $g=3.3\times10^6$, and every 1000 time units g is reduced by 22%. For every value of g, ΔV is calculated by averaging over 200 time units and is displayed in a log-log plot. The slopes of the straight lines are -1 and -0.25. For large values of g, $\Delta V\propto 1/g$, in agreement with Eq. (32). For smaller values of g, the slope becomes less negative, in agreement with Eq. (31). In this regime, almost every decrease in g changed the clustering pattern in the network, resulting in large fluctuations in the value of ΔV for adjacent values of g.

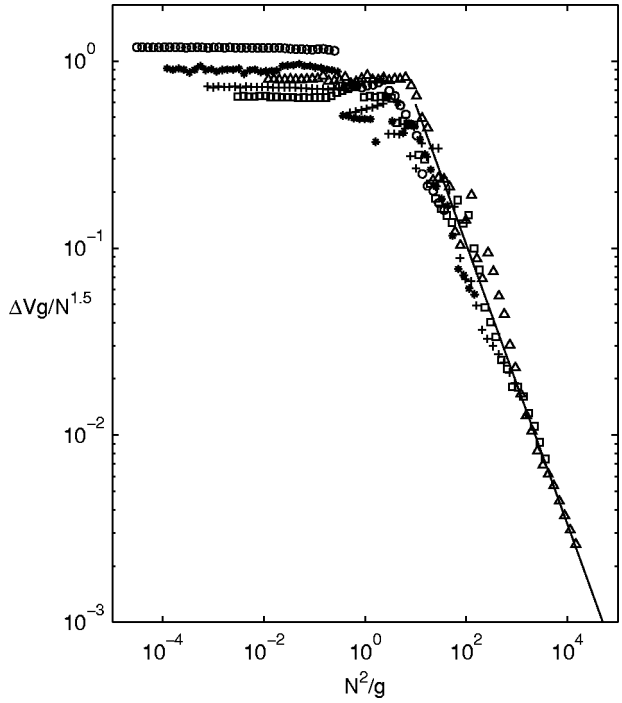

FIG. 9. The scaling behavior of a one-dimensional nearest neighbor lattice model. Equation (24) is simulated with $g_{ij}=g(\delta_{i,j+1}+\delta_{i,j-1})$ and periodic boundary conditions for $N=10$ (circles), 20 (stars), 50 (crosses), 100 (boxes), 200 (triangles). ΔV is calculated for different values of g in the same paradigm as in Fig. 8. $\Delta V g N^{-3/2}$ is shown as a function of N^2/g. The straight line has a slope of -0.75. Note that ΔV can be approximated by the scaling law of Eq. (33). The fluctuations from the scaling in the $N^2/g\ll 1$ regime result from the fact that the initial conditions are random, thus resulting in different patterns of clustering for each value of N, which result in a different value of $F(0)$.

This behavior is valid in a finite, but large systems in the regime of $g\ll N^2$. In contrast, when $g\gg N^2$, the lower limit of the integral dominates the result and Eq. (30) becomes

$$\Delta V\propto\frac{1}{g}N^{3/2} \tag{32}$$

in agreement with Eq. (15). This behavior is illustrated in Fig. 8, where the dynamics of Eq. (24) is simulated in a one-dimensional lattice model of $N=200$, with nearest neighbor connectivity and periodic boundary conditions. ΔV is plotted as a function of g. The slopes of the two straight lines are -1 and $-\frac{1}{4}$. In the $g\gg N^2$ regime, ΔV is inversely proportional to g, in agreement with Eq. (32). As g decreases, the slope of ΔV vs g decreases, which is consistent with Eq. (31). In contrast to the smooth behavior in the $g\gg N^2$ regime, when $g\ll N^2$ there are large fluctuations in the value of ΔV for adjacent values of g. These fluctuations result from the fact that in this regime, changing g resulted in changing the clustering pattern, thereby changing the value of $x^k(\omega)$. Since ΔV is proportional to $x^k(\omega)$, the changing of the clustering pattern for adjacent values of g generates the ''noise'' in Fig. 8.

Equation (30) can be used to derive a scaling function for ΔV, which holds in the intermediate regime,

$$\Delta V=\frac{1}{g}N^{3/2}F\left(\frac{N^2}{g}\right), \tag{33}$$

where $F(Z\to 0)=O(1)$ and $F(Z\to\infty)\propto Z^{-3/4}$. This scaling behavior is illustrated in Fig. 9, where Eq. (24) is simulated for one dimensional lattice models with different values of N and g in the same paradigm as in Fig. 8. $\Delta V g N^{-3/2}$ is shown as a function of N^2/g. The straight line has a slope of $-\frac{3}{4}$. The simulations results show that, indeed, ΔV can be described by the scaling law as in Eq. (33). Note, however, that different initial conditions result in different clustering patterns. Since the initial conditions are random, they differ in the simulations for the different values of N, and therefore the value of $F(0)$ is slightly different for the different N.

IV. DISCUSSION

A. Summary of the main results

Electrical coupling is often considered to synchronize and thus homogenize the activity of electrically coupled net-

works. This paper, together with previous works, shows that electrical coupling can destabilize the homogeneous rest state and break the spatiotemporal symmetry in the network. This paper deals with the mechanism for the generation of oscillations by electrical coupling of identical nonoscillating excitable elements. The basic concept is that the interaction of the membrane potential with the internal variables suppresses the tendency of the latter to oscillate. The electrical coupling diminishes the suppression capability of the potential in the heterogeneous direction, thereby destabilizes the homogeneous fixed point and gives rise to oscillations via a Hopf bifurcation. Thus, the homogeneous fixed point is unstable even for arbitrarily large coupling strengths, where the membrane potentials of the different cells oscillate almost in-phase. This mechanism leads to a surprising, but simple experimental prediction: affixing the membrane potential of an isolated cell to its resting potential value (voltage clamp) will generate oscillations of the internal variables, which will generate oscillations in the current needed for the clamping.

When the bifurcation is normal, the frequency of the oscillations near the bifurcation point is solely dependent on the properties of the isolated cell and is independent of the architecture. In contrast, the spatial structure of the oscillations is determined by the network architecture, which, in general, leads to either in-phase or antiphase oscillations.

Particular emphasis was given to the limit of strong coupling, with different network architectures. When the coupling strength is infinite, the network dynamics has many attractors, which are characterized by the grouping of the different cells into several clusters. When the coupling is strong but not infinite, the clustering solutions are retained, but the spatial fluctuations of the membrane potential depend on the network architecture. In the fully connected networks, the fluctuations in the membrane potential are inversely proportional to the coupling strength. In contrast, in the one-dimensional lattice model, we have shown that there are two asymptotic regimes, depending on the way of taking the limit of large network and strong coupling.

In general, our mechanism characterizes a large family of dynamical systems. For reasons of clarity, we have discussed it here in a less general form, where the number of internal variables is two, the dynamics of the membrane potential is linear, and the membrane potential is linearly coupled to one of the internal variables. However, since much of the analysis is done by linearizing near the fixed point, the generalization to more complex models is straightforward.

B. Comparison to other mechanisms

Another model in which electrical coupling of identical nonoscillating cells generates oscillations was proposed by Sherman and Rinzel [12]. In their model, in addition to a stable fixed point, stable oscillations of the membrane potentials exist in a restricted range of values of the electrical coupling. The bifurcation in their model is far from the homogeneous fixed point, and thus the fixed point remains stable for all coupling strengths. Ermentrout and Lewis [5] proposed a continuum model of population dynamics, in which oscillatory behavior is dependent on diffusion of one of the species. In a discrete version of their model, an increase in the coupling strength generates oscillations via a Hopf bifurcation. However, these oscillations are limited to a strict regime of coupling strengths, and in the limit of strong coupling the homogeneous fixed point is stable. This difference results from the fact that the fixed point of the ''internal variables,'' Eq. (2) is stable in their model, but is unstable in our mechanism.

A mechanism for generation of oscillations by electrical coupling, which relies on heterogeneity in the properties of the coupled cells, has been proposed [13,14]. In this mechanism, although the isolated cells do not oscillate, when they are strongly coupled they behave similarly to an isolated cell with ''average'' properties. This ''average'' cell is oscillatory. Thus, similar to our model, oscillations in this case are present even for arbitrarily strong coupling. However, in the heterogeneous model, the internal variables lock in a unique fashion to the oscillating potential and therefore they oscillate in phase. It is the heterogeneity in the properties of the different cells that enables a moderate current flow even when the membrane potentials of the cells are very similar, and thus generates the oscillatory behavior. In contrast, our mechanism does not rely on heterogeneity in the isolated cells properties. The heterogeneity is generated by a spontaneous symmetry breaking, in which the internal variables of the different cells lock to the common membrane potential in a different manner.

C. Relevance to biological systems

Several biological systems including the inferior olive, the locus coeruleus, the β-pancreatic cells, and the aortic smooth muscle cells exhibit oscillations that depend in some way on electrical coupling. Network oscillations in these systems are usually synchronized and in-phase, which is consistent with our mechanism, but not with the homogeneous models described above. Our proposed mechanism may be applicable to some of these systems. Of particular importance are the possible clinical implications of our dynamical mechanism. It has been suggested that in Creutzfeldt-Jakob disease, fusion of neuronal processes, particularly dendrites, may lead to abnormal electrotonic coupling between the cells, generating periodic EEG discharges [15]. In addition, we have recently applied our mechanism to explain the phenomenon of ''alcohol withdrawal tremor.'' Long-term abuse of alcohol, which blocks the gap junctions, may induce a strengthening of the electrical coupling in the inferior olive. During the first days of abstinence, the excessive electrical coupling causes exaggerated synchronized membrane potential oscillations, which manifest as a large amplitude tremor [16].

This mechanism can be realized in different biophysical models. Elsewhere [7] we have proposed that the internal variables are the calcium concentrations in the cytoplasm of cells and in cellular organelles; e.g., endoplasmatic reticulum and mitochondria. Instability of these internal variables arises from the calcium-induced calcium release current. An increase in the calcium concentration in the cytoplasm triggers the opening of calcium channels in the organelles, in

which the calcium concentration is much higher, causing a flow of calcium from the organelles to the cytoplasm. This positive feedback loop is terminated with the depletion of calcium from the organelles [17]. The stability of the isolated cell results from the interaction of the calcium concentration in the cytoplasm with the membrane via the calcium dependent potassium current and the voltage dependent calcium current. Alternatively, this mechanism can be realized in a network of two-compartment neurons. One compartment is an excitable soma whose parameters play the role of the internal variables, and a passive dendrite whose membrane potential plays the role of V. The isolated soma of the neurons is oscillatory but its interaction with the dendrite dampens these oscillations, yielding nonoscillating cells. Electrical coupling via dendro-dendritic gap junctions in this model leads to sustained oscillations [8].

A growing number of studies in recent years have demonstrated that electrical coupling in the central nervous system is far more common than was previously considered. It has been described in cortical [18] and cerebellar inhibitory neurons [19] as well as in the hippocampus [20] and locus coeruleus [21]. In all these studies it has usually been assumed that electrotonic coupling serves as a synchronizing device, or as a fast excitatory pathway. In this work we suggest that in addition, electrical coupling can serve as a generator of oscillatory activity. Although one would expect that oscillatory activity, which is associated with electrotonic coupling, will be rather homogeneous, we have shown that it does not decrease the flexibility of the network. On the contrary it furnishes it with a wide range of dynamic features.

ACKNOWLEDGMENTS

We thank Bard Ermentrout, David Hansel, John Rinzel, and Yosef Yarom for their helpful discussions, and Maoz Shamir for his valuable comments on the draft. This work was supported by the Yeshaya Horowitz Association and the Israel Science Foundation.

[1] A.M. Turing, Philos. Trans. R. Soc. London, Ser. B **237**, 37 (1952).
[2] L. Edelstein-Keshet, *Mathematical Models in Biology* (McGraw-Hill, New York, 1988), Chap. 11.
[3] S. Smale, *Lectures on Mathematics in the Life Sciences* (the American Mathematical Society, Providence, RI, 1974).
[4] K. Kishimoto, K. Mimura, and K. Yoshida, J. Math. Biol. **18**, 213 (1983).
[5] B. Ermentrout and M. Lewis, Bull. Math. Biol. **59**, 533 (1997).
[6] R. Dermietzel and D.C. Spray, Trends Neurosci. **16**, 186 (1993).
[7] Y. Loewenstein, Y. Yarom, and H. Sompolinsky, Proc. Natl. Acad. Sci. U.S.A. **98**, 8095 (2001).
[8] J. Loewenstein, H. Sompolinsky, and Y. Yarom, *Society for Neuroscience Abstract 25* (Society for Neuroscience, Washington, D.C., 1999).
[9] J. Rubin and D. Terman, J. Math. Biol. **41**, 513 (2000).
[10] C. van Vreeswijk, Phys. Rev. E **54**, 5522 (1996).
[11] J. Guckenheimer and P. Holmes, *Nonlinear Oscillations, Dynamical Systems, and Bifurcations of Vector Fields* (Springer-Verlag, New York, 1983), Chap. 2.
[12] A. Sherman and J. Rinzel, Proc. Natl. Acad. Sci. U.S.A. **89**, 2471 (1992).
[13] Y. Manor, J. Rinzel, I. Segev, and Y. Yarom, J. Neurophysiol. **77**, 2736 (1997).
[14] J.H.E. Cartwright, Phys. Rev. E **62**, 1149 (2000).
[15] R.D. Traub and T.A. Pedley, Ann. Neurol. **10**, 405 (1981).
[16] Y. Loewenstein, Mol. Psychiatry **7**, 129 (2002).
[17] A. Goldberter, G. Dupont, and M. Berridge, Proc. Natl. Acad. Sci. U.S.A. **87**, 1461 (1990).
[18] J.R. Gibson, M. Beierlin, and B.W. Connors, Nature (London) **402**, 75 (1999).
[19] P. Mann-Metzer and Y. Yarom, J. Neurosci. **19**, 3298 (1999).
[20] A. Draguhn, R.D. Traub, D. Schmitz, and J.G.R. Jefferys, Nature (London) **394**, 182 (1998).
[21] M.J. Christie, J.T. Williams, and R.A. North, J. Neurosci. **9**, 3584 (1989).